

# Exhaust energy conversion by thermoelectric generator: Two case studies

M.A. Karri\*, E.F. Thacher, B.T. Helenbrook

Department of Mechanical and Aeronautical Engineering, PO Box 5725, Clarkson University, Potsdam, NY 13699, USA

## ARTICLE INFO

### Article history:

Received 28 October 2008

Received in revised form 29 September 2010

Accepted 6 October 2010

Available online 20 November 2010

### Keywords:

Exhaust energy recovery  
Waste-heat  
Fuel savings  
Thermoelectric generator  
Vehicle modeling

## ABSTRACT

This study reports predictions of the power and fuel savings produced by thermoelectric generators (TEG) placed in the exhaust stream of a sports utility vehicle (SUV) and a stationary, compressed-natural-gas-fueled engine generator set (CNG). Results are obtained for generators using either commercially-available bismuth telluride ( $\text{Bi}_2\text{Te}_3$ ) or quantum-well (QW) thermoelectric material. The simulated tests are at constant speed in the SUV case and at constant AC power load in the CNG case. The simulations make use of the capabilities of ADVISOR 2002, the vehicle modeling system, supplemented with code to describe the thermoelectric generator system. The increase in power between the QW- and  $\text{Bi}_2\text{Te}_3$ -based generators was about three times for the SUV and seven times for the CNG generator under the same simulation conditions. The relative fuel savings for the SUV averaged around  $-0.2\%$  using  $\text{Bi}_2\text{Te}_3$  and  $1.25\%$  using QW generators. For the CNG case the fuel savings was around  $0.4\%$  using  $\text{Bi}_2\text{Te}_3$  and around  $3\%$  using QW generators. The negative fuel gains in the SUV were caused by parasitic losses. The power to transport the TEG system weight was the dominant parasitic loss for the SUV but was absent in the CNG generator. The lack of space constraint and the absence of parasitic loss from the TEG system weight in the CNG case allowed an increase in the TEG system size to generate more power.

© 2010 Elsevier Ltd. All rights reserved.

## 1. Introduction

New thermoelectric materials show the promise of reaching significantly higher values of the thermoelectric figure of merit,  $Z$ , and thus higher efficiencies and power densities. Some of the most promising materials are quantum-well structured materials [1] and skutterudites [2]. Theoretical analyses have shown that quantum-well (QW) structured materials could possibly increase  $Z$  by an order of magnitude relative to the bulk material [3]. Hi- $Z$  technologies has successfully made one and two-couple devices [4,5] and shown  $ZT$  values (where  $T$  is the average operating temperature) of up to 4 [6] compared to most current materials which are around 1. This has the potential of roughly proportionally increasing the conversion efficiency of thermoelectric devices.

In our previous paper [7], we showed that it is difficult to make an automotive thermoelectric exhaust generator that generates enough power to overcome the rolling resistance penalty associated with the device. This is especially true at low vehicle speeds when the amount of power in the exhaust stream is reduced. The purpose of this paper is to examine the impacts that new materials may have on the viability of vehicle exhaust waste heat recovery with particular emphasis on how new materials affect the behavior of the entire system. Specifically, we examine the impact of QW materials compared to  $\text{Bi}_2\text{Te}_3$  materials. QW materials were chosen

as representative of the potential of new materials, but skutterudites also show significant potential. For more information on skutterudite modules and their optimization, the reader is referred to the work of El-Genk and co-workers [8–10].

There has been a significant amount of research done examining waste heat recovery. Hendricks [11–15] has created a model of a generic generator and subsequently examined its optimization under various conditions and with varying materials. In general, these studies focus on the thermoelectric system including the heat exchangers but do not examine impacts on a vehicle system. Rowe and co-workers have concentrated on the modules themselves, doing fundamental work examining their optimization for waste heat recovery [16–20]. Additional work in optimization of modules for waste heat recovery are given by Chen et al. [21], Crane and Jackson [22], and Wu [23] and a discussion of the impacts of novel materials on modules are given in [24]. The work of Crane [25] includes some components of a vehicle system by accounting for power losses due to the fan and fluid pump required for the coolant system, but this study was done only using Bismuth–Telluride modules.

In the following, we try to assess the impact of new materials on the entire vehicle system including the coolant system, exhaust back pressure effect, and parasitic loss due to weight. Fairbanks [26] gave an overview of the application and manufacturing of QW thermoelectric materials to vehicles, and Willigan [27] discussed the fabrication of QW thermoelectric material for vehicle waste heat recovery. In this work, we investigate the potential benefits

\* Corresponding author. Tel.: +1 315 268 3753; fax: +1 315 268 6695.

E-mail address: [karrima@clarkson.edu](mailto:karrima@clarkson.edu) (M.A. Karri).

**Nomenclature**

$A$	heat transfer area or cross-sectional area of thermocouple leg	$\eta$	efficiency
$C_1, C_2$	coolant loss coefficient parameters	$\gamma$	leg aspect ratio
$c_p$	specific heat at constant pressure	$\mu$	rolling resistance
$I$	total current of the generator	$\nu$	kinematic viscosity
$j$	Colburn factor	$\rho$	electrical resistivity or density
$K$	thermal conductance	<b>Subscript</b>	
$k$	thermal conductivity or pressure loss coefficient	0	baseline case
$l$	length of thermocouple leg	$B$	blow-down
$LHV_{AF}$	lower heating value of the air–fuel mixture	$c$	cold junction
$\dot{m}$	mass flow rate	$D$	driveline
$N_c$	number of couples	$E$	engine
$N_p$	number of unit generators in parallel	$e$	exhaust side
$N_s$	number of unit generators in series	$f$	coolant side property
$p$	pressure	$G$	alternator electrical generation
$Q$	volumetric flow rate	$h$	hot junction
$R$	electrical resistance	$j$	module index
$S$	fuel savings	$L$	load
$T$	temperature	$oc$	open circuit
$\bar{U}$	average heat transfer coefficient	$P$	coolant pumping
$V$	voltage	$T$	TEG
$v$	vehicle velocity	<b>Acronyms</b>	
$W$	weight	CNG	compressed natural gas generator
$\dot{W}$	power	PCHX	pre-cooling heat exchanger
$Z$	figure of merit	PCU	power conditioning unit
<b>Greek</b>		QW	quantum well
$\alpha$	Seebeck coefficient	SUV	sports utility vehicle
$\Delta$	change in quantity	TEG	thermoelectric generator

of QW thermoelectric materials and try to understand how much of a benefit these materials will have in two practical applications. The paper compares predictions of the power produced and fuel saved when exhaust energy is recovered using a thermoelectric generator (TEG) composed of one of two materials: QW or commercially available  $\text{Bi}_2\text{Te}_3$ . The comparison is made for a sports utility vehicle (SUV) (Case 1) and a stationary compressed natural gas generator (CNG) (Case 2). To allow performance comparisons, simulations were performed for each case with no TEG installed (baseline case), with a TEG installed that used the commercially available  $\text{Bi}_2\text{Te}_3$  modules, and with a TEG installed that used modules employing QW based thermoelectric material. The paper begins with a description of the development of a simulation code followed by a description and results for the two cases.

## 2. Simulation code development

The simulation code consists of a model of the TEG combined with ADVISOR 2002, which, when originally obtained, was free, non-commercial, and downloadable. ADVISOR is a MATLAB® and Simulink®-based vehicle simulator written at National Renewable Energy Laboratory and documented in [28]. ADVISOR was used to model the needed vehicle inputs, such as fuel use, exhaust flow rates and temperatures, alternator efficiency, etc. This was coupled to a model of the TEG system we developed which has been validated [29] by comparing it to the test results reported in [7] and is described herein.

### 2.1. Thermoelectric generator

The TEG model is based on an actual generator that was built using the HZ20,  $\text{Bi}_2\text{Te}_3$ -based, thermoelectric module sold by

Hi-Z Technology, Inc (Hi-Z) [30]. This generator was tested in a 1999 General Motors Sierra pick-up truck [7] and is shown in Fig. 1 without exterior insulation, inlet and outlet transition pieces, and outer casing. As shown in the figure, the tested generator incorporated sixteen HZ20 modules connected in series. Eight of the modules were on each side of a central exhaust heat exchanger made of carbon steel. Cooling was provided by a pair of aluminum heat exchangers, one on each side. Thin aluminum oxide wafers electrically isolated the thermocouple circuits in the modules from the heat exchangers. The contact surfaces on each side of these wafers were covered with thermal grease and the entire assembly was clamped together with a 200-psi cold preload using the shown preload subassembly.

To model this device we assumed thermal symmetry with respect to the orthogonal vertical and horizontal planes as shown in Fig. 1, and that extraneous heat losses could be neglected because of the insulation and casing mentioned previously. The symmetry planes divide the generator into four zones extending over its length. Each zone contains four modules and may be divided into four, equal-sized sections containing a single module, as shown in Fig. 2.

To model this section, we neglect axial conduction in the metal and assume that the hot and cold junction temperatures,  $T_{h,j}$  and  $T_{c,j}$  over module  $j$  are uniform. A steady-state energy balance on the coolant heat-exchanger section considering convection in the fluid and conduction heat transfer to the module surface gives

$$c_{p,f,j} T_{f,j} - c_{p,f,j+1} T_{f,j+1} - \frac{\bar{U}_{f,j} A_f}{\dot{m}_f} (T_{c,j} - \bar{T}_{f,j}) = 0, \quad (1)$$

where  $\bar{U}_{f,j}$  is the average overall heat transfer coefficient for the coolant heat exchanger for this section,  $A_f$  is the coolant side heat transfer area for this section,  $\dot{m}_f$  is the mass flow rate of the coolant

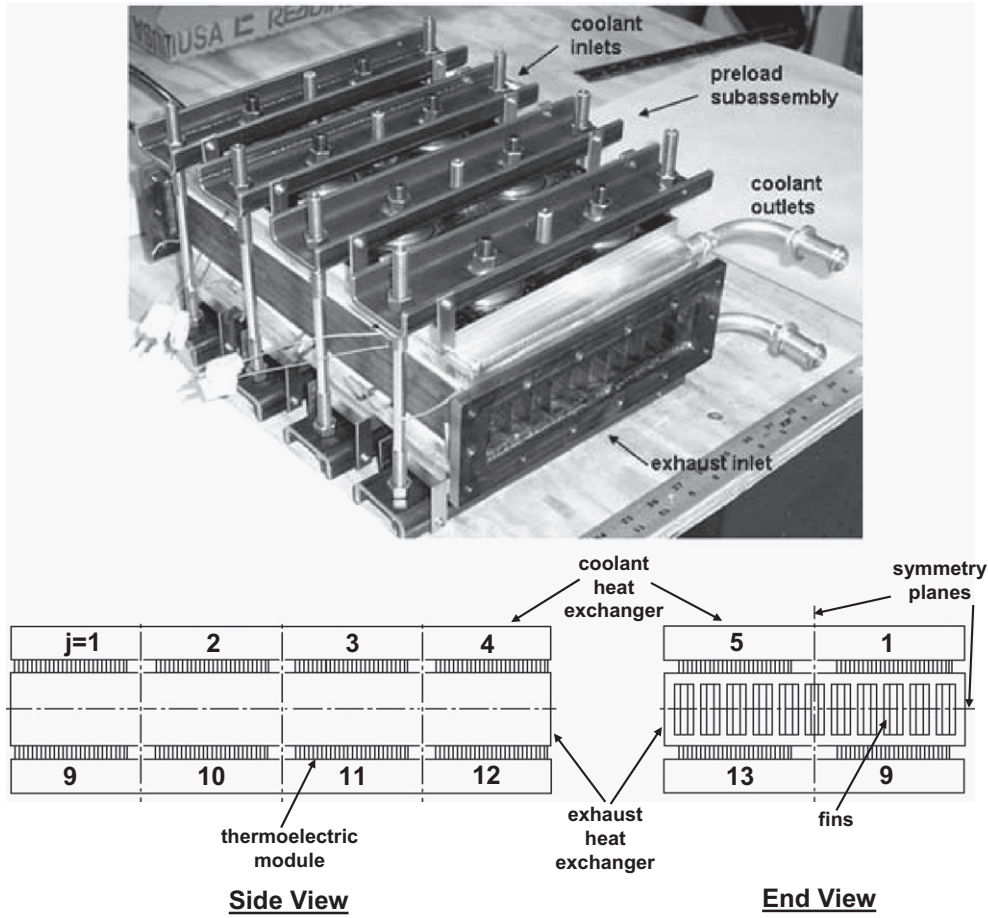


Fig. 1. Tested TEG (courtesy Hi-Z) and layout schematic.

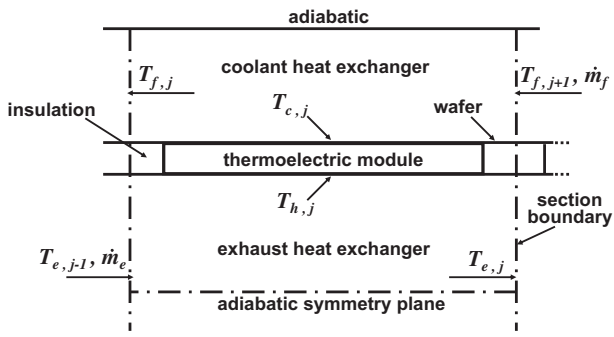


Fig. 2. Side view of a module section.

through the section,  $c_{p,f,j}$  is the specific heat of the coolant evaluated at  $T_{f,j}$ , and  $\bar{T}_{f,j}$  is the average bulk coolant temperature for this section defined by

$$\bar{T}_{f,j} = \frac{1}{2} (T_{f,j} + T_{f,j+1}). \quad (2)$$

Similarly, for the exhaust heat exchanger segment

$$c_{p,e,j} T_{e,j} - c_{p,e,j-1} T_{e,j-1} - \frac{\bar{U}_{e,j} A_e}{\dot{m}_e} (\bar{T}_{e,j} - T_{h,j}) = 0, \quad (3)$$

where the variables have definitions similar to those in Eq. (1).

Balancing the energy flow in and out of the module gives

$$\bar{U}_{e,j} A_e (\bar{T}_{e,j} - T_{h,j}) - \bar{U}_{f,j} A_f (T_{c,j} - \bar{T}_{f,j}) - \dot{W}_j = 0. \quad (4)$$

$\dot{W}_j$ , the power generated by the module, is

$$\dot{W}_j = IV_j = I(V_{oc,j} - IR_j), \quad (5)$$

where  $I$  is the total current of the generator,  $V_j$  is the module's voltage,  $V_{oc,j}$  is the module's open circuit voltage, and  $R_j$  is the electrical resistance of the module.  $R_j$  is given by

$$R_j = N_c \gamma \rho(\bar{T}_j), \quad (6)$$

where  $N_c$  is the number of (series-connected) couples in the module,  $\rho(\bar{T}_j)$  is the resistivity of a couple evaluated at the average of the junction temperatures, and  $\gamma$  is  $\frac{l}{A}$ , the aspect ratio of the legs of a couple, assumed uniform over the generator.  $l$  and  $A$  are the leg length and cross-sectional area respectively. The module's open circuit voltage,  $V_{oc,j}$ , is

$$V_{oc,j} = \alpha_j (T_{h,j} - T_{c,j}), \quad (7)$$

where  $\alpha_j$  is the Seebeck coefficient of the module.  $\alpha_j$  is given by

$$\alpha_j = N_c \alpha(\bar{T}_j), \quad (8)$$

where  $\alpha(\bar{T}_j)$  is the Seebeck coefficient of a couple evaluated at the average of the junction temperatures. The generator current,  $I$ , is

$$I = \frac{V_{oc}}{R_T + R_L} = \frac{\sum_{j=1}^{16} V_{oc,j}}{\sum_{j=1}^{16} R_j + R_L}, \quad (9)$$

where  $V_{oc}$  is the total open circuit voltage of the generator,  $R_T$  is the electrical resistance of the thermoelectric generator, and  $R_L$  is the load resistance.

A heat balance on the hot surface of the module as derived in [31] is

$$\bar{U}_{ej}A_e(\bar{T}_{ej} - T_{hj}) - K_j(T_{hj} - T_{cj}) - \alpha_j T_{hj}I + \frac{1}{2}I^2 R_j = 0, \quad (10)$$

where  $K_j$  is the thermal conductance of the module.  $K_j$  is given by

$$K_j = N_c \frac{k(\bar{T}_j)}{\gamma}, \quad (11)$$

where  $k(\bar{T}_j)$  is the thermal conductivity of a couple evaluated at the average of the junction temperatures.

Finally, the power of the thermoelectric generator is

$$\dot{W}_T = I^2 R_L. \quad (12)$$

## 2.2. Thermoelectric module properties

The two types of module models used in the calculations were based on QW and  $\text{Bi}_2\text{Te}_3$  materials. The  $\text{Bi}_2\text{Te}_3$  based thermoelectric module properties were obtained from the Hi-Z HZ20 product brochure [30]. The HZ20 module consists of 71 thermocouples connected in series electrically. The module properties were evaluated using voltage, power, and efficiency curves based on the analysis developed in [29]. However, the experimental power production [7] was less than the predicted power production for the TEG using standard HZ20 module data [30] and experimental module surface temperatures [7]. The Seebeck coefficient of the HZ20 module was reduced to improve agreement with the experimental power production. The relative change in magnitude of the Seebeck coefficient was about 8% at  $T_h - T_c$  of 50 °C to 29% at 300 °C. This adjustment resulted in a reduction of  $Z$  by a factor of between 1.2 and 1.7 over this temperature range. The studies of the  $\text{Bi}_2\text{Te}_3$  material-powered generator, which we name the HZ20M, were made with this adjustment.

The QW module properties were based on p-type and n-type Seebeck coefficient, resistivity, and thermal conductivity material data, which was furnished by Hi-Z [32]. These properties were given as a function of temperature. Fig. 3 shows the resistivity of the QW material as function of temperature as compared to  $\text{Bi}_2\text{Te}_3$ . The Seebeck coefficient and thermal conductivity were relatively insensitive to temperature. The p-type QW material had  $\alpha \approx 1031 \mu\text{V}/^\circ\text{C}$  and  $k \approx 0.5 \text{ W}/(\text{cm } ^\circ\text{C})$  as compared to  $199 \mu\text{V}/^\circ\text{C}$  and  $0.014 \text{ W}/(\text{cm } ^\circ\text{C})$  for the p-type  $\text{Bi}_2\text{Te}_3$  material. For the n-type

QW material, the values were  $\alpha \approx -1104 \mu\text{V}/^\circ\text{C}$  and  $k \approx 0.13 \text{ W}/(\text{cm } ^\circ\text{C})$  as compared to  $-175.4 \mu\text{V}/^\circ\text{C}$  and  $0.01 \text{ W}/(\text{cm } ^\circ\text{C})$  for  $\text{Bi}_2\text{Te}_3$ . Note however that the HZ20M properties were not derived from these material properties but rather from actual module performance tests as discussed above. Fig. 4 shows a comparison of the  $Z$  factors of the two modules. As the QW materials have not been produced as a module, to reduce the number of variables and to provide a comparison to the HZ20M, the number of couples and total area for the QW module, the HZQW, were assumed to be equal to that of the HZ20M. Fig. 4 shows that using the QW modules results in a factor of increase in  $Z$  ranging from 3 to 6.7.

## 2.3. Fluid properties

Both the exhaust and coolant fluid properties were evaluated as a function of temperature. The density and specific heat at constant pressure of the exhaust gas were found from ideal gas mixture theory. The relative amounts of pure components in the exhaust mixture were determined using molar analysis for a given fuel type and the air–fuel mass ratio obtained from the engine maps in the ADVISOR. The dynamic viscosity of the gas was found using an equation for gas mixtures [33]. For the coolant properties in Case 1, an engine coolant composed of 50% by volume solution of ethylene glycol in water, was used. Its properties were evaluated using the Prestone Antifreeze coolant properties [34]. In Case 2, compressed liquid water at atmospheric pressure was the coolant.

## 2.4. Heat exchangers and heat transfer coefficients

The overall heat transfer coefficients,  $\bar{U}_e$  and  $\bar{U}_f$ , include the forced convection in the heat exchangers, conduction through the fins, and the contact resistance between the heat exchangers and the thermoelectric modules. The exhaust heat exchanger was an offset-strip fin design made of carbon steel. The geometry of the fins is described in [29]. The design was close to that for which correlations for the Colburn factor and friction factor were reported in [35] to agree with experimental data to within 20% for a range of fin geometry. These correlations determine the Colburn factor and friction factor coefficients as a function of the specific geometry of the heat exchanger as well as the Reynolds number of the flow. Thus, these parameters were evaluated as a function of the Reynolds number of the exhaust flow.

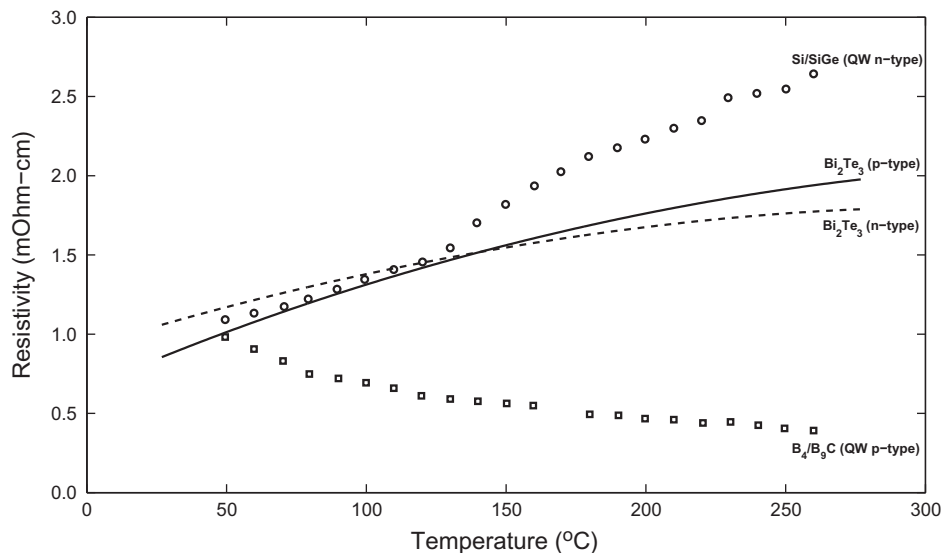


Fig. 3. QW material and  $\text{Bi}_2\text{Te}_3$  material electrical resistivities (courtesy Hi-Z).

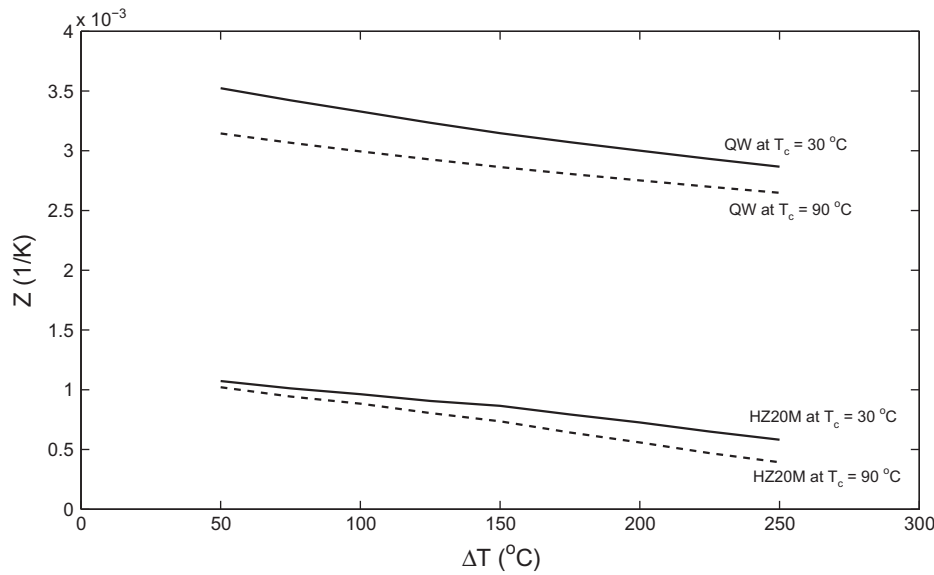


Fig. 4. QW and HZ20M Z values.

The coolant heat exchanger consisted of six, parallel, rectangular flow channels milled in a block of aluminium. The Reynolds number of the flow based on the hydraulic diameter of these slots ranged from about 1300 at 48.3 km/h to about 3000 at 112.7 km/h [29]. Thus it ranged from the laminar to transitional region. However, because of the flow disturbance imparted by upstream flow devices such as the elbows, tees, fittings, and manifolds, we assumed the flow to be turbulent. The Dittus–Boelter correlation [36] was therefore employed to calculate the heat transfer coefficient.

## 2.5. Solution strategy

Eqs. (1), (3)–(5), and (10) combined with Eq. (9), were simultaneously solved by the multi-dimensional Newton–Raphson method to find the four unknown temperatures in each section,  $T_{c,j}$ ,  $T_{h,j}$ ,  $T_{e,j}$ ,  $T_{f,j}$ ,  $j = 1, 2, \dots, 16$ , and thus to calculate the performance of the generator, principally its power production. The analyses were carried out at matched load,  $R_L = R_T$  for both cases. The QW cases were also run at optimum leg aspect ratio,  $\gamma$ . The method of determining optimum  $\gamma$  will be discussed in a subsequent section.

## 2.6. Unit generator

The design shown in Fig. 1 was taken as a “unit generator”. The number of unit generators was varied depending on the exhaust source. In the fixed engine-generator study, Case 2, for example, the number of unit generators was increased because there was more exhaust flow available and there were no particular space and weight constraints, as there were in the vehicle of Case 1. In Case 2,  $N_p$  identical parallel lines, each parallel line consisting of  $N_s$  unit generators in series, were fed by the exhaust and coolant flows. As a result, each parallel line received  $\frac{1}{N_p}$  of the total flow. This approach simplified the modeling and also kept the work grounded in a model that agreed sufficiently well with the experiment [29].

## 3. Case 1: sports-utility vehicle

In this section, we examine the impact of thermoelectric power generation on an SUV cruising at various speeds. We start with a

description of the system design followed by a discussion about the modeling approach, determining of optimum coolant flow rate and thermoelectric leg aspect ratio, and concluding with the discussion of the results.

### 3.1. System design

Fig. 5 illustrates the system schematic for Case 1. This scheme was based on the installation reported in [7] in which the TEG was located downstream of the catalytic converters as shown in Fig. 5 and the intervening exhaust piping was insulated. Vazquez et al. [37] and motor vehicle industry contacts advised against locating TEGs between the exhaust manifold and the catalytic converters because of possible slowing of heating of catalytic converters, resulting in an increased pollutant release. Furthermore, the temperature limits of the module also limit the possible positions for the TEG. Both modules can be placed just downstream of the catalytic converter without exceeding their temperature limitations.

Engine coolant was chosen to cool the TEG instead of air cooling because the larger heat transfer coefficient available with liquid cooling allows smaller heat exchangers to be used and does not require fans at low or zero vehicle speed. Because the TEG is tapped into the coolant system through the cabin heat hoses, the temperature of the coolant supplied to the TEG is actually the highest in the coolant system. The most desirable point to tap into the coolant system is just after the radiator because this is the coldest point in the system. However, the operation of the by-pass and thermostat valves could then prevent coolant from flowing to the TEG. In the experimental testing [7], a pre-cooling heat exchanger (PCHX) was placed upstream of the TEG. Its purpose was to reduce the TEG coolant inlet temperature to levels more representative of the radiator outlet. The effect of the PCHX on the coolant temperature drop was modeled by determining the temperature drop across the PCHX at different vehicle speeds from the test results [7]. This temperature drop was deducted from the engine coolant temperature, from ADVISOR, to determine the coolant inlet temperature to the TEG.

As shown in Fig. 5, the electrical output of the TEG was connected to the vehicle’s electrical bus through a power conditioning unit (PCU). The PCU was essentially a direct-current-to-direct-current converter functioning as a buck regulator, matched the generator’s output voltage to the approximately 14.5 V potential of the

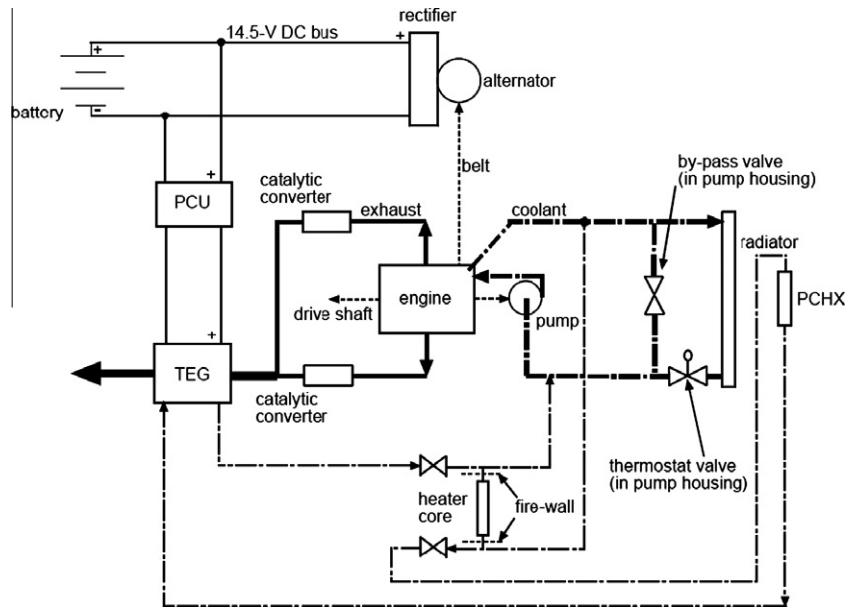


Fig. 5. System design Case 1.

vehicle's direct current bus and kept the TEG operating at its maximum power point. A PCU efficiency of 88% [38] was used in the simulation. The alternator efficiency was 50% [39], typical of belt-driven units.

### 3.2. Modeling approach

Fig. 6 illustrates the data flow for the system model. The system model consisted of three main components: (1) ADVISOR to model

the vehicle system, (2) the TEG system model, previously described, and (3) the coolant system model. ADVISOR did not contain a model for the engine coolant system, therefore a model of it was formulated (discussed subsequently). The basic input parameters to the TEG model, exhaust flow rate and inlet temperature and coolant flow rate and inlet temperature, were obtained from ADVISOR and the coolant system models. The output parameters, electrical power and associated parasitic losses, were fed back to ADVISOR which then predicted the fuel consumption.

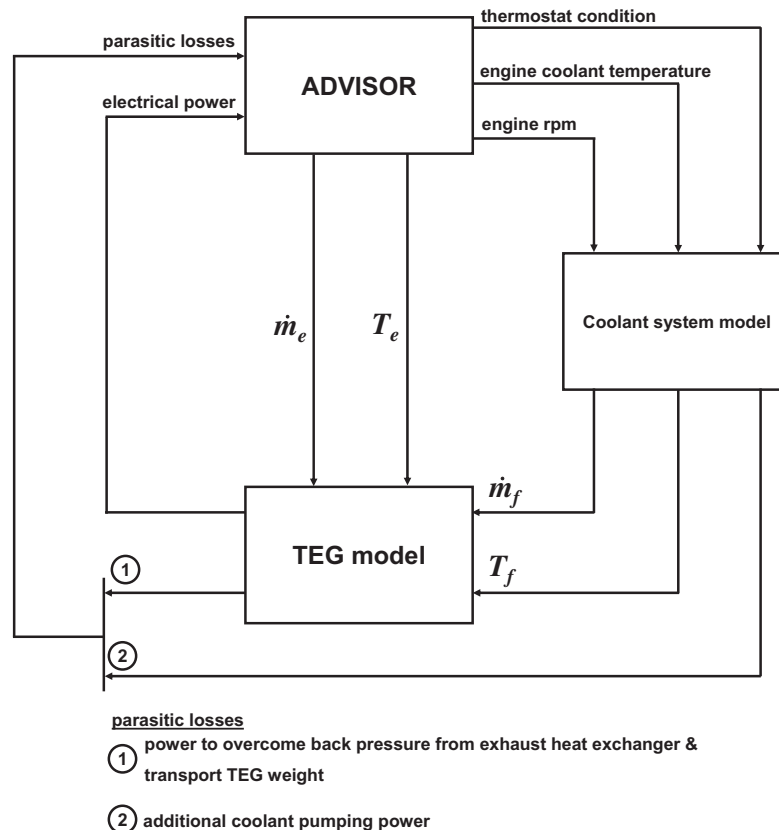


Fig. 6. Modeling approach Case 1.

### 3.2.1. Engine model

The engine model chosen from ADVISOR's library was a 1991 Dodge Caravan 3.0 L (102 kW) SI engine with a torque scaling factor of 1.95 applied to yield an exhaust temperature and mass flow rate similar to those of the test vehicle [7]. The coolant thermostat set point for this engine was modified from the default value in ADVISOR to give coolant temperatures similar to those measured during testing [7].

### 3.2.2. Coolant system model

This model predicted: the coolant flow rate through the TEG, the additional pumping power needed to cool the TEG, and the change in flow rates through the other components of the coolant system. The model was based on the coolant system in the truck used for testing the TEG [7]. The measurements taken during those experiments and additional data supplied by General Motors in [40,41] were used in the model development and the verification reported by [29]. Fig. 7 is a flow diagram of the system with resistor symbols representing loss coefficients. The surge tank is not shown. The main flow loop is through the pump and engine and then through four parallel paths consisting of the radiator by-pass, the radiator, the heater, and the TEG. The model is bi-polar in that it treats only the case when the thermostat valve is fully open or fully closed. Sufficient data to model the intermediate condition could not be obtained. However, the former condition will exist during cruising at constant speed, the state adopted in Case 1.

The coolant was assumed incompressible and changes in potential and kinetic energy were neglected. The pressure losses for any fluid element,  $\Delta p$ , was assumed to obey

$$\Delta p = \rho_f k Q^2, \quad (13)$$

where  $Q$  is the volumetric flow rate through the element and  $\rho_f$  is the coolant density. The loss coefficients,  $k$ , were assumed to depend only on the Reynolds number. Because it was difficult to precisely define the hydraulic diameter and thus the Reynolds number in some locations, the data was fit using the following alternative form, where  $\nu$  is the kinematic viscosity,

$$k = C_1 \left( \frac{Q}{\nu} \right)^{C_2}. \quad (14)$$

Karri [29], reports the various values of  $C_1$  and  $C_2$  used to fit the experimental data for each flow resistance. Reference [29] showed that Eq. (14) worked well for most flow elements except in the engine case, where the scatter in the data was large. However, the pre-

dictions of the system model agreed well with the available measurements.

GM provided data relating engine speed to flow and pressure drop for various components of the unmodified system, but a pump characteristic curve at any given engine speed was not available. Therefore, because the flow rates through the TEG were low relative to the flow rates through the other components of the coolant system, we assumed the variation in the pump head caused by the additional flow to the TEG could be neglected. The pressure drop across the TEG and PCHX,  $\Delta p_T$  and the flow rate through the TEG,  $Q_T$ , could then be found using

$$\Delta p_T = \rho_f k_T Q_T^2 = \Delta p - \rho_f k_E Q^2, \quad (15)$$

where  $k_E$  and  $k_T$  are the loss coefficient for the flow through the engine and TEG loop respectively.  $\Delta p$  is the total pressure head provided by the pump and  $Q$  is the total flow rate. To determine  $Q$ , the loss coefficients of the system were used to determine an equivalent system loss coefficient using standard methods [42] and then Eq. (13) was used. This process was performed iteratively to allow for the variation of the loss coefficients with Reynolds number.

### 3.3. Parasitic power losses

The parasitic engine shaft power changes caused by the TEG were due to coolant pumping, exhaust blow-down work, and rolling resistance.

#### 3.3.1. Coolant pumping power

The parasitic coolant pumping power increase is given by

$$\Delta \dot{W}_p = \dot{W}_p - \dot{W}_{p0},$$

where  $\Delta \dot{W}_p$  is the parasitic pumping power,  $\dot{W}_{p0}$  is the pumping power in the baseline case (no TEG), and  $\dot{W}_p$  is the pumping power with the TEG. For Case 1, as a full description of the coolant system was available, this expression was used to directly evaluate the additional coolant pumping power. For Case 2, the coolant system was generically defined and the parasitic pumping power was estimated by dividing the hydraulic power associated with the TEG circuit by the pump efficiency

$$\Delta \dot{W}_p \approx \frac{\rho_f k_T Q_T^3}{\eta_p}, \quad (16)$$

where  $\eta_p$  is the pump efficiency. A comparison of these two approaches for Case 1 showed that  $\left( \frac{\rho_f k_T Q_T^3}{\eta_p} \right)$  tends to predict a parasitic pumping power about 10.5% greater than that of  $(\dot{W}_p - \dot{W}_{p0})$ .

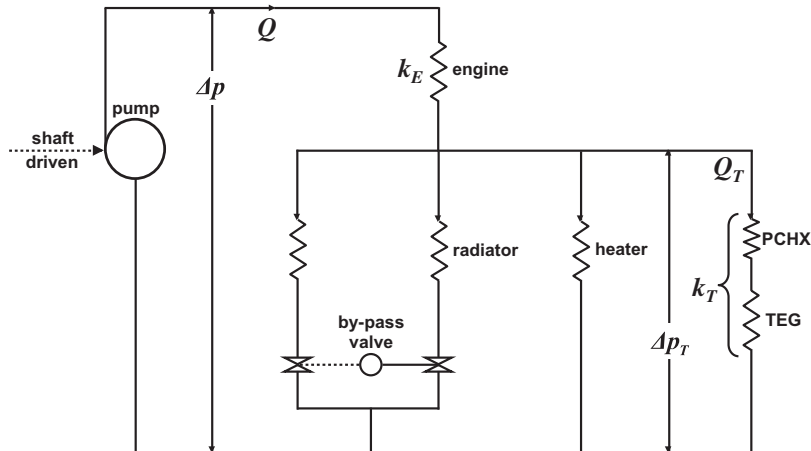


Fig. 7. Coolant system.

### 3.3.2. Blow-down power

The blow-down power is the power required for the engine to drive the exhaust through the exhaust system. The magnitude of this power changes because of the flow resistance introduced by the TEG exhaust heat exchanger. The blow-down power change caused by the altered exhaust back-pressure can be calculated as

$$\Delta \dot{W}_B = k_e \frac{\dot{m}_e^3}{\rho_e^2} - k_{e0} \frac{\dot{m}_{e,0}^3}{\rho_{e,0}^2}, \quad (17)$$

where  $\dot{m}_e$  is the exhaust mass flow rate,  $\rho_e$  is the exhaust density, and  $k_e$  is a lumped exhaust loss coefficient which includes the losses from the exhaust pipes, muffler, catalytic converter, and TEG. A negative or positive change in blow-down work will depend on the relative magnitude of the changes in  $\dot{m}_e$  and  $k_e$ . If there is a decrease in shaft power due to the gains produced by the TEG,  $\dot{m}_e$  will decrease and the blow-down work may decrease in spite of the increased  $k_e$ . This was observed during the testing reported by [7].

In the baseline case, the effect of blow-down power is implicitly incorporated through the engine efficiency map used in ADVISOR. To include the additional effect of the TEG, the power required to force the flow through the TEG is treated as if it is supplied by an external fan. The power for this fan is assumed to be supplied directly from the engine shaft. In this case, the additional blow-down work for the TEG is given by

$$\dot{W}_{B,T} = k_{e,T} \frac{\dot{m}_e^3}{\rho_e^2}, \quad (18)$$

where  $k_{e,T}$  is the exhaust loss coefficient determined from the heat exchanger friction factor and we have assumed that the (purely conceptual) fan used to supply this power is 100% efficient.

### 3.3.3. Power to transport TEG system weight

The parasitic power to transport the total weight of the TEG system is given by

$$\Delta \dot{W}_D = \frac{\mu_D W_T v}{\eta_D}, \quad (19)$$

where  $\mu_D$  is the rolling resistance coefficient,  $W_T$  is the weight of the TEG system,  $v$  is the velocity of the vehicle, and  $\eta_D$  is the driveline transmission efficiency. The driveline transmission efficiency accounts for the losses in the linkages between the drive shaft and

the wheels and is provided by ADVISOR. The driveline transmission efficiency depends on vehicle speed but is roughly constant at about 0.9. ADVISOR also provides a rolling resistance coefficient of 0.012, and the mass of TEG used in the testing was 40 kg.

### 3.4. Optimizing TEG coolant flow rate

Increasing the coolant flow rate, for fixed exhaust and coolant inlet temperatures, decreases the cold junction temperature consequently increasing the junction temperature difference and the power produced by the modules. But an increase in coolant flow rate will also increase the pumping power proportional to the cube of the flow rate, as shown by Eq. (16). The optimum flow rate is that which gives the largest difference between the TEG output power and the pumping power required to circulate coolant through the TEG at a particular engine rotational speed. In the experiment, the coolant flow rate was set by opening or closing butterfly valves in the TEG coolant loop. In this section, we theoretically determine the optimal coolant flow rate (and thus the  $k_T$  value) for maximizing the net power from the TEG.

Studies were performed to estimate the optimum coolant flow rates at various vehicle speeds under fully open and closed thermostat conditions. Fig. 8 shows results obtained for the conditions shown in Table 1. The power generated by the TEG, the power required to pump the coolant through the TEG, the net power produced by the TEG, and the change in total flow rate and change in flow rates through the heater, by-pass, and the radiator as a function of coolant flow through the TEG are shown. The coolant flow rate that maximized the net power produced by the TEG was about  $6.3 \times 10^{-5} \text{ m}^3/\text{s}$ . At this flow rate, the changes in flow rate through the other components of the coolant system were less than 5%. At 112.7 km/h the optimum was at about  $1.9 \times 10^{-4} \text{ m}^3/\text{s}$  (not shown). Based on these studies, an intermediate value of  $k_T$  was chosen that resulted in a flow rate ranging from  $1.5 \times 10^{-4}$  to  $2.8 \times 10^{-4} \text{ m}^3/\text{s}$  over all test speeds.

### 3.5. Optimum aspect ratio

An increase in the aspect ratio of the thermoelectric legs will decrease the module thermal conductance and increase its electrical resistance. These competing effects produce a power maximum

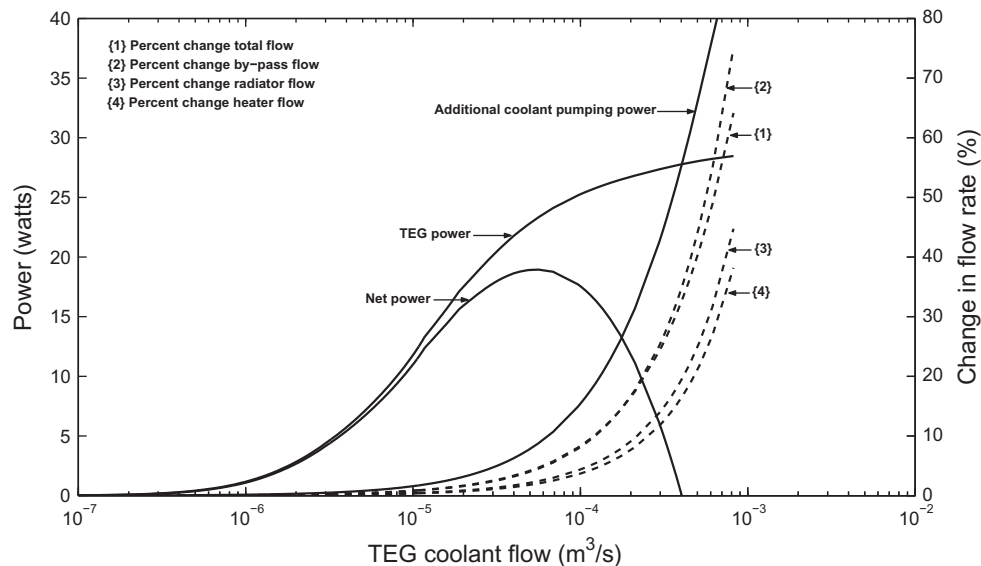


Fig. 8. Optimal coolant flow analysis for Case 1 at 48.3 km/h vehicle speed.

**Table 1**

Data used in the optimal coolant flow analysis shown in Fig. 8.

Variable	Value
Ambient temperature	21.1 °C
Vehicle speed	48.3 km/h
Vehicle electrical load	550 W
Exhaust mass flow rate	0.0142 kg/s
Exhaust inlet temperature	413.50 °C
Coolant inlet temperature	88 °C
Thermostat condition	Fully open
Module	HZ20M

**Table 2**

Data used in optimizing  $\gamma_{QW}$  for Case 1.

Vehicle speed (km/h)	$\dot{m}_e$ (kg/s)	$T_e$ (°C)	$Q_T$ (kg/s)	$T_f$ (°C)
48.3	0.0154	426.4	$1.5 \times 10^{-4}$	79.63
80.5	0.0286	496.6	$2 \times 10^{-4}$	77.96
112.7	0.0520	562.8	$2.9 \times 10^{-4}$	76.61

at a particular aspect ratio. Consequently,  $\gamma_{QW}$  was studied for both cases to find the ratio that maximized the total power production.

The data used in the optimization is given in Table 2. The exhaust inlet temperature and mass flow rate were obtained from the baseline simulation results and the coolant inlet temperature and flow rate were obtained from the simulation results using HZ20M module properties. Fig. 9 shows the results. Maximum powers of 117.3, 245.7, and 459.3 W corresponding to 48.3, 80.5, and 112.7 km/h were obtained at the aspect ratios shown. An aspect ratio of  $5158 \text{ m}^{-1}$  was used for all of the simulations using the HZQW in Case 1. The consequential reduction in the optimum power at 48.3 and 80.5 km/h was about 16.4 and 8.3 W (14% and 3.4%), respectively.

For comparison, the HZ20M legs have a cross-sectional area,  $A$ , of  $0.248 \text{ cm}^2$  ( $0.498 \text{ cm} \times 0.498 \text{ cm}$ ) and are  $0.267 \text{ cm}$  long, giving  $\gamma_{\text{HZ20M}} = 107.6 \text{ m}^{-1}$ . Assuming cross-sectional area,  $A$ , for power-optimized HZQW legs equal to that of HZ20M would require a leg length of  $12.8 \text{ cm}$ . An alternative design procedure would be to fix the volume of the thermoelectric material equal to that of the HZ20M. Requiring the same leg volume as in HZ20M gives

$$A_{QW} = \sqrt{\frac{\gamma_{\text{HZ20M}}}{\gamma_{QW}}}, A_{\text{HZ20M}} = \sqrt{\frac{107.6}{5158}} 0.248 = 0.036 \text{ cm}^2. \quad (20)$$

The legs of the power-optimized HZQW module would then be  $1.83 \text{ cm}$  long with a cross-sectional area,  $A$ , of about  $0.036 \text{ cm}^2$  ( $0.189 \text{ cm} \times 0.189 \text{ cm}$ ). (Note that Hi-Z, is in the process of building QW modules having 49 couples, with a leg length of about  $1.27 \text{ cm}$  and a cross-sectional area of about  $0.258 \text{ cm}^2$  [43] giving  $\gamma = 492 \text{ m}^{-1}$ .)

### 3.6. Results

#### 3.6.1. TEG power

The power produced by the TEG at vehicle speeds of 48.3, 80.6, and  $112.7 \text{ km/h}$  is shown in Fig. 10. In this figure and in the next two figures, the vertical ranges show the effect of electrical load on the system. At each of the speeds, simulations corresponding to electrical loads of 550, 900, and  $1250 \text{ W}$  were performed. This effect was small relative to the variation in power with vehicle speed. The power increased with speed mainly because the exhaust mass flow rate and inlet temperature increased with speed while the coolant inlet temperature was relatively constant. The power extracted using HZQW modules was approximately three times the power extracted using HZ20M modules.

#### 3.6.2. Fuel savings

An theoretical expression for the relative fuel savings will be useful in discussing the results. Assuming that the engine exhaust contains no liquid water, an energy balance on the engine gives:

$$\dot{W}_E = \eta_E \dot{m}_e \text{LHV}_{AF}, \quad (21)$$

where  $\dot{W}_E$  is the engine shaft power,  $\eta_E$  is the engine shaft efficiency, and  $\text{LHV}_{AF}$  is the lower heating value of the air–fuel mixture at inlet conditions. The engine shaft power is used (in general) for driveline propulsion, coolant pumping, blow-down power, alternator electric power generation  $\dot{W}_G$ , as well as other possible loads from the air-conditioning unit and the cooling fan which we assume constant for this analysis.

$$\dot{W}_E = \dot{W}_D + \dot{W}_P + \dot{W}_B + \dot{W}_G + \dot{W}_{\text{other}}. \quad (22)$$

The portion of the shaft power required to drive the alternator is

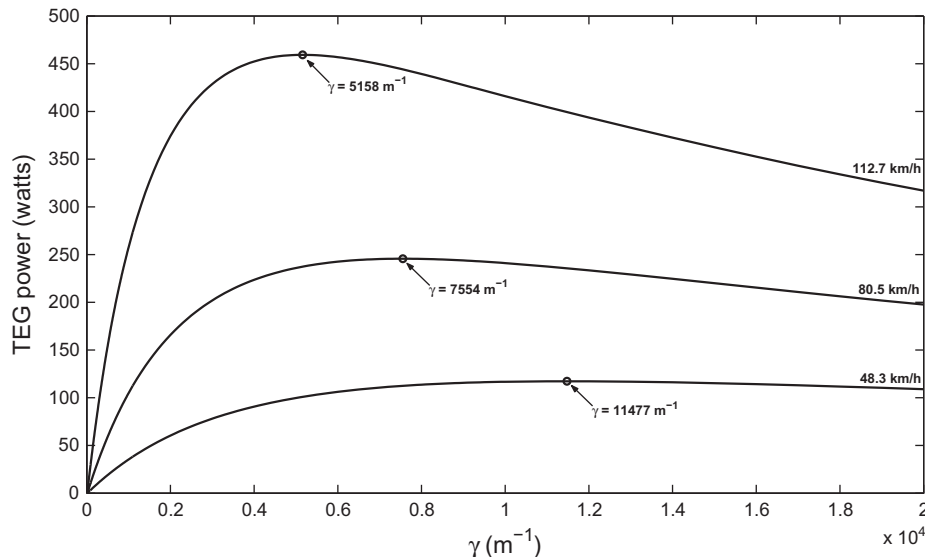


**Fig. 9.** SUV  $\gamma_{QW}$  optimization.

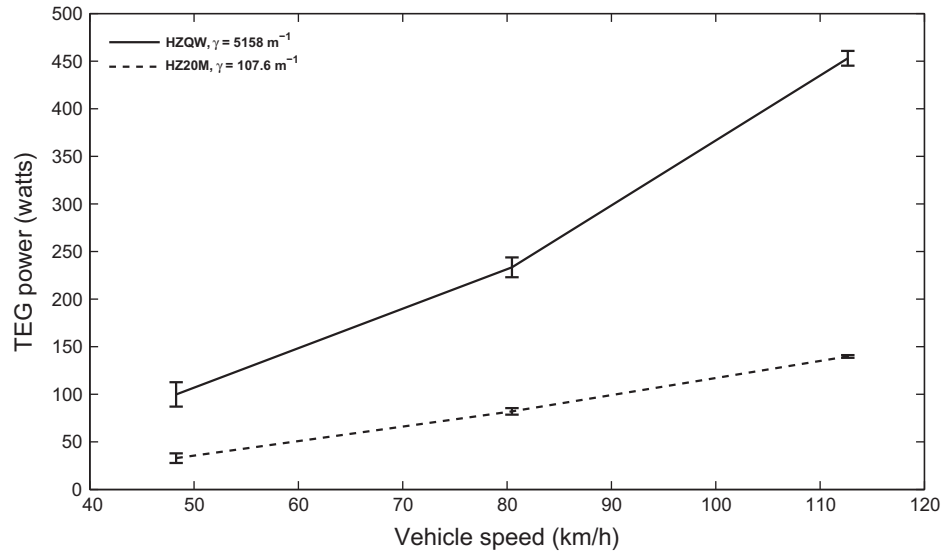


Fig. 10. TEG power production Case 1.

$$\dot{W}_G = \frac{\dot{W}_L}{\eta_G}, \quad (23)$$

where  $\dot{W}_L$  is the electrical load and  $\eta_G$  is the efficiency of the alternator. Using Eqs. (21)–(23) and taking the difference between the baseline case and the case with the TEG gives an equation for the fuel savings ratio,  $S$ ,

$$S = -\frac{\Delta \dot{m}_e}{\dot{m}_e} = -\frac{\Delta \dot{W}_D + \Delta \dot{W}_P + \Delta \dot{W}_B}{\dot{W}_{E0}} + \frac{\eta_{PCU} \dot{W}_T}{\eta_G \dot{W}_{E0}}, \quad (24)$$

where  $\eta_{PCU}$  is the PCU efficiency and we have assumed that the electrical load remains constant but is offset by the power supplied by the TEG. Eq. (24) shows that the fuel savings depend on three dimensionless ratios: (1) the loss ratio, which is the ratio of the total parasitic loss to the baseline shaft power, (2) the efficiency ratio, which is the ratio of the PCU efficiency to the alternator efficiency, and (3) the power ratio, which is the ratio of the TEG power to the baseline shaft power. We will use this equation to help explain the fuel savings.

Fig. 11 shows fuel savings. Positive fuel savings were attained at all the vehicle speeds using HZQW module. The maximum fuel savings of about 1.5% was obtained at a vehicle speed of 112.7 km/h using this module. However, negative fuel gains were registered at vehicle speeds of 48.3 and 80.6 km/h using the HZ20M module. Using Eq. (24) and assuming no parasitic losses, for the HZQW-TEG power varying from 100 to 450 W the relative fuel savings should be about 2–2.3% and for the HZ20M-TEG power varying from 33 to 140 W the relative fuel savings should be about 0.68 to 0.83%. However, as shown in Fig. 11 under both cases the relative fuel savings is significantly lower because of parasitic effects of the TEG on the vehicle system.

A comparison of the TEG shaft power to its associated parasitic losses powers is shown in Fig. 12. To base the comparison to a standard point of reference, the TEG power was converted into its respective shaft powers as shown in Eq. (24). The parasitic blow-down power does not include the entire exhaust system because loss coefficients, for example for the exhaust pipe and muffler, were not available. Only the effect of the flow resistance from

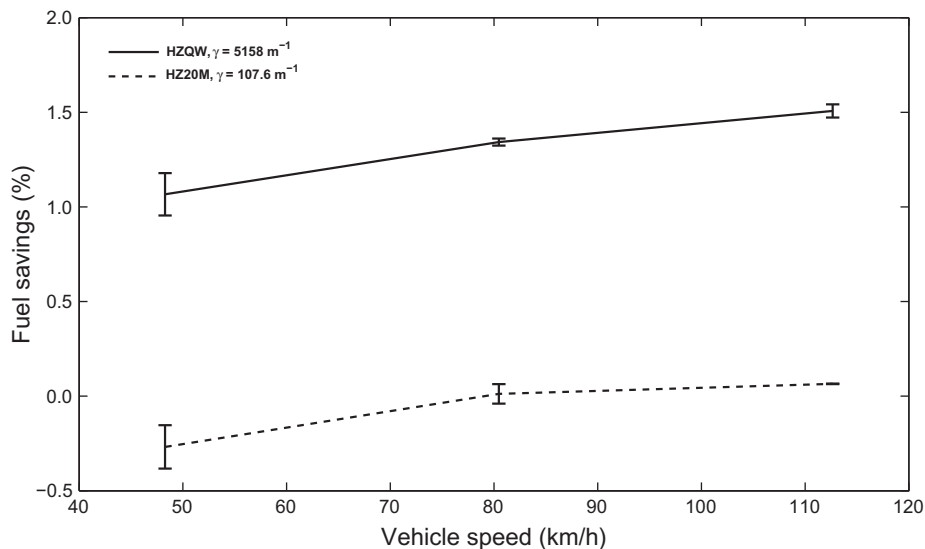


Fig. 11. Fuel savings Case 1.

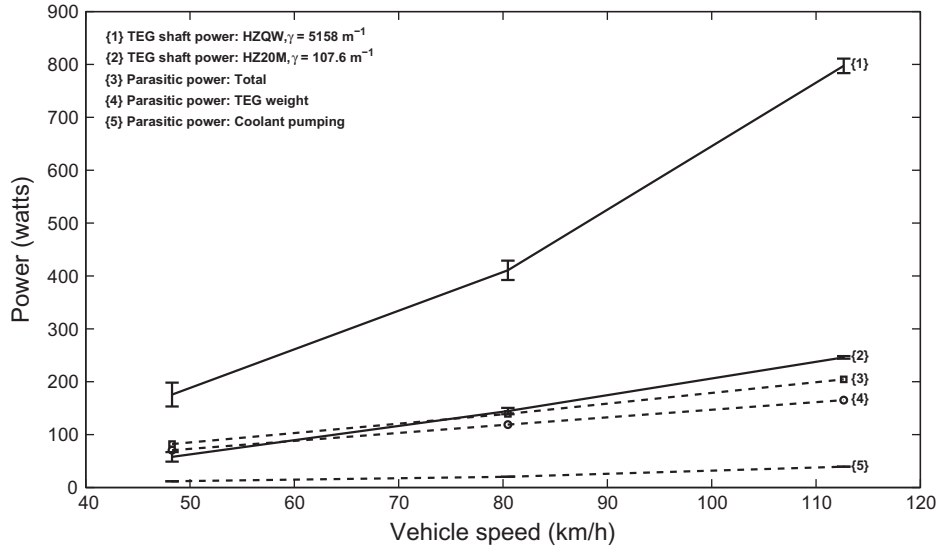


Fig. 12. Parasitic losses Case 1.

the TEG is included as shown in Eq. (18). Fig. 12 shows that the total parasitic loss exceeded the power produced by the TEG at lower vehicle speeds for the HZ20M. This resulted in a fuel consumption increase compared to the base case, as shown in Fig. 11. The dominant parasitic loss is the power to transport the TEG system weight which increases with vehicle speed. The difference in weight for the unit TEG due to the change in modules from HZ20M to HZQW will depend on the leg geometry of the QW module. For example, the power-optimized QW module with a leg cross-sectional area,  $A_{QW}$ , of about  $0.036 \text{ cm}^2$  would have a weight of about 24 g [44]. We do not know the feasibility of these designs from a manufacturing standpoint. In contrast, the weight of the HZ20M module is about 115 g [30] and the total weight of the 16 HZ20 modules, used in the tested TEG, was about only 4.6% of the total TEG weight which was dominated by the heat exchangers. This implies that the change in thermoelectric material will not result in a significant change in the parasitic loss associated with the TEG weight.

The coolant pumping power and the blow-down power are less significant. The coolant pumping power is almost independent of the vehicle speed because the coolant system by-pass valve maintains an approximately constant pressure drop across the heater core even as the engine *rpm* changes [41]. Therefore the resulting flow and pressure drop through the TEG coolant loop are approximately independent of vehicle speed. The coolant pumping power was the same for the two modules. The blow-down power is nearly the same between the two cases as well, primarily because there was not a large change in exhaust mass flow rate. For the cases in which the TEG produces a net positive power, what is shown is actually a worst-case representation. The blow-down power in the remainder of the exhaust system decreases relative to the baseline because of the reduced exhaust gas flow rates.

### 3.6.3. Energy budget

Table 3 compares the energy budget for the HZQW and HZ20M. The following are evaluated in the table:

- Maximum possible exhaust power that can be extracted,

$$\dot{W}_{e,max} = \dot{m}_e(c_{p_{e,i}}T_{e,i} - c_{p_{e,f,i}}T_{f,i}), \quad (25)$$

where  $\dot{W}_{e,max}$  is the total possible exhaust power that can be extracted,  $c_{p_{e,i}}$  is the specific heat of the exhaust evaluated at  $T_{e,i}$ ,  $T_{e,i}$

Table 3

Energy budget Case 1.

Vehicle speed	(km/h)	48.3	80.5	112.7
<b>HZQW</b>				
$\dot{W}_{e,max}$	(kW)	6.27	14.25	30.46
$\dot{W}_e$	(kW)	2.26	3.63	5.31
Effectiveness	(%)	36.12	25.46	17.43
TEG power	(kW)	0.100	0.233	0.453
Heat rejected to coolant	(kW)	2.16	3.39	4.86
TEG efficiency	(%)	4.41	6.44	8.53
<b>HZ20M</b>				
$\dot{W}_{e,max}$	(kW)	6.37	14.51	31.01
$\dot{W}_e$	(kW)	2.59	4.15	6.21
Effectiveness	(%)	40.80	28.63	20.04
TEG power	(kW)	0.033	0.082	0.140
Heat rejected to coolant	(kW)	2.56	4.07	6.07
TEG efficiency	(%)	1.26	2.00	2.25

is the exhaust inlet temperature into the TEG,  $c_{p_{e,i}}$  is the specific heat of the exhaust evaluated at  $T_{f,i}$ , and  $T_{f,i}$  is the coolant inlet temperature into the TEG.

- Actual exhaust energy extracted,

$$\dot{W}_e = \dot{m}_e(c_{p_{e,i}}T_{e,i} - c_{p_{e,o}}T_{e,o}), \quad (26)$$

where  $\dot{W}_e$  is the exhaust energy extracted,  $c_{p_{e,o}}$  is the specific heat of the exhaust evaluated at  $T_{e,o}$ , and  $T_{e,o}$  is the exhaust outlet temperature from the TEG.

- The effectiveness of TEG is the ratio of exhaust energy extracted to maximum possible exhaust energy that can be extracted.
- Power generated by the TEG.
- Exhaust energy rejected to coolant.
- TEG efficiency, the ratio of power generated by the TEG to exhaust energy extracted.

Table 3 shows the TEG efficiency increased by a factor of about 3.2–3.8 because of the change from the HZ20M to the HZQW. Thus, because the HZQW rejects less heat, a lower coolant flow rate could be used. This would reduce the parasitic pumping losses and further increase the gains associated with switching to QW material.

Table 3 shows the effectiveness of the unit TEG using HZ20M modules is about 41%, 29%, and 20% at 48.3, 80.5, and 112.7 km/h

respectively. This indicates that the exhaust energy at higher speeds was underutilized. The effectiveness of the HZQW decreases to 36%, 25%, and 17% at 48.3, 80.5, and 112.7 km/h respectively. This highlights the fact that the switch to better thermoelectric materials needs to be augmented with better heat exchanger designs. A possible scenario would be to increase the plan area of the TEG system, so that more modules could be employed, thereby increasing the power generated and exhaust energy extracted. However, the size of the TEG system was constrained by the limited space in the underbody. Additionally, an increase in system size would increase the system weight and consequently the rolling resistance parasitic loss.

To summarize, the application of QW and  $\text{Bi}_2\text{Te}_3$  based TEG to the SUV has been studied. The power generated by the TEG using HZQW was about 100–400 W. This should result in a fuel savings of about 2–2.3%. However, the fuel savings decreased by about 30%, primarily due to the rolling resistance parasitic loss. The exhaust energy was underutilized because of space limitations, especially at higher vehicle speeds.

#### 4. Case 2: natural gas engine generator

In this section, we examine the impact of the thermoelectric power generation on a stationary, compressed-natural-gas-powered generator at various electrical loads.

##### 4.1. System design

Fig. 13 illustrates the system schematic for Case 2. The absence of parasitic loss from TEG system weight, the lack of space constraint, and the higher exhaust flow, allowed us to use more than one unit TEG. The TEG stack was located downstream of the catalytic converter for the reasons given earlier.

As shown in Fig. 13, the electrical output of the TEG stack is connected to the AC generator's electrical bus through a PCU. The PCU

for this study, besides matching the TEG stack output to the AC generator voltage and tracking the maximum power point of the TEG stack, converts the TEG stack output from direct to alternating current. The PCU's efficiency was assumed to be 88%. The AC generator performance data was obtained from the specification sheet for the John Deere Power Tech 6068H Diesel engine for generator set applications. This AC generator was chosen based on the load capabilities of the CNG engine. The AC generator has an electrical output of 124–143 kW operating at a frequency of 60 Hz and an efficiency of about 88–92% [45].

##### 4.2. Modeling approach

Fig. 14 illustrates the data flow for the system model. This model consists of three main components: (1) engine torque calculator, (2) CNG model, and (3) TEG stack model. The engine torque calculator determines the torque required at the engine shaft for a given AC generator load, efficiency, and shaft speed. The CNG model calculates the fuel usage, exhaust mass flow rate and temperature and other variables based on the required torque and engine speed, and the TEG stack model is similar to the TEG system model which was previously described. Since ADVISOR is designed as a vehicle analysis tool, changes were made to the CNG model to account for the stationary characteristics of Case 2. The engine used in this case study was a John Deere 8.1 L (186 kW) CNG SI engine, the only CNG engine available in the library of ADVISOR. The exhaust mass flow rate from this engine was about five times that of the SUV in Case 1 at 80.5 km/h.

##### 4.3. Optimization

The optimum number and arrangement of TEGs was found by calculating the net maximum power from the TEG stack under various combinations of parallel and series configurations using the HZQW. The power from the TEG stack was determined using an

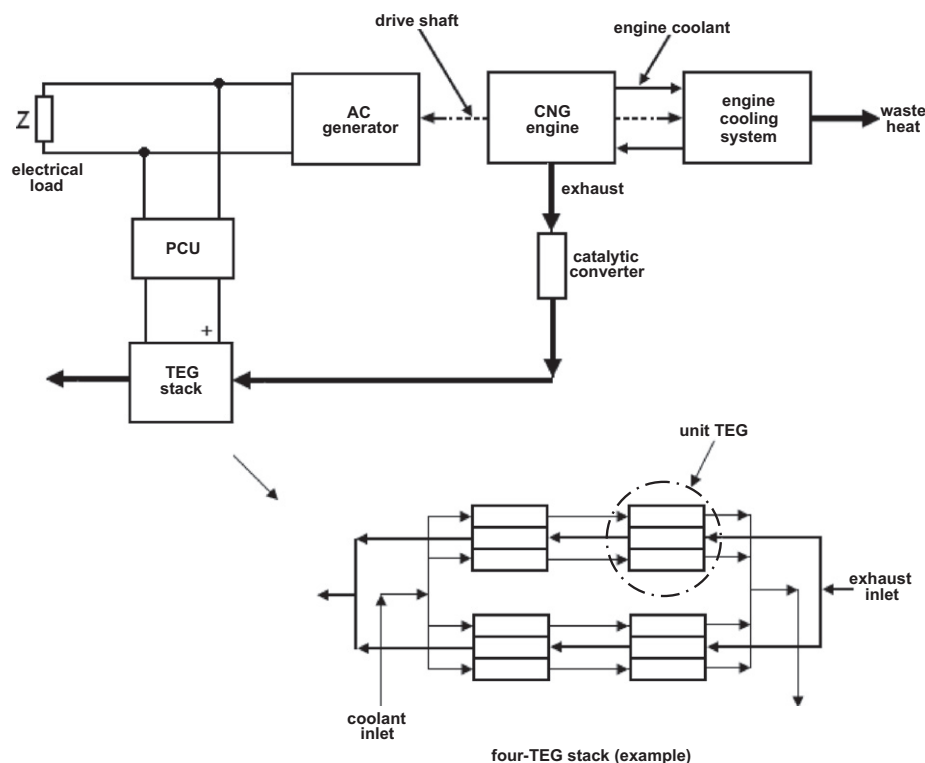


Fig. 13. System design Case 2.

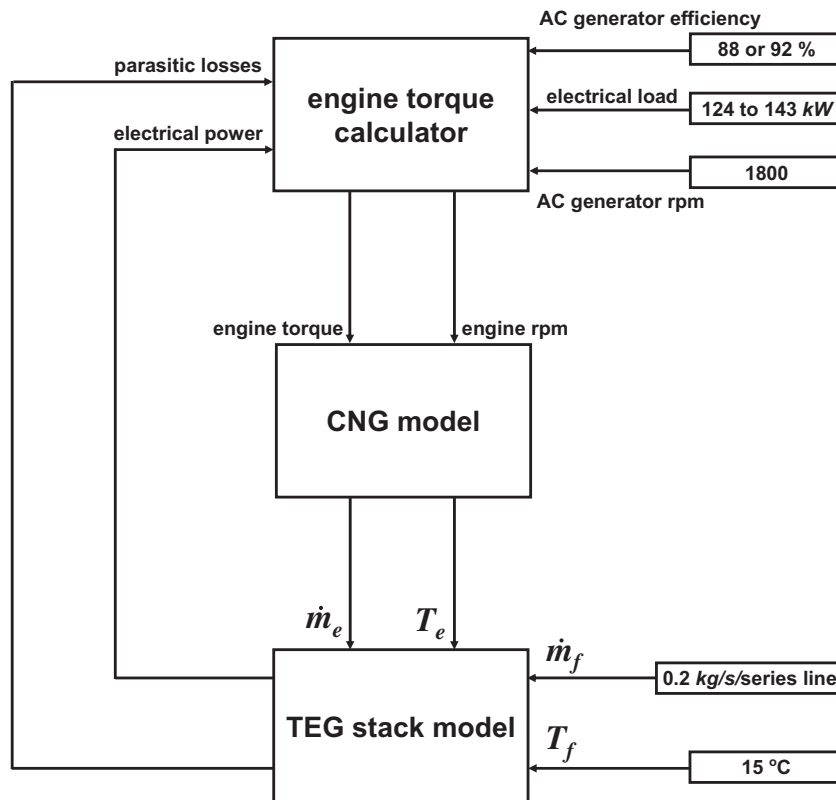


Fig. 14. Modeling approach Case 2.

optimum aspect ratio,  $\gamma$ , found for each stack configuration. Case 2 losses consisted of coolant pumping power and blow-down power. The unit TEGs in series were arranged in a counter-flow arrangement. The flow pattern for a  $2 \times 2$  configuration is shown in Fig. 13. The exhaust flow and inlet temperature conditions were obtained from the baseline simulations. The total exhaust mass flow rate was 0.163 kg/s and the exhaust inlet temperature was 469 °C. We assumed that there was a continuous supply of water from city mains or cooling towers to cool the TEG stack. The coolant flow through each of the series lines and the inlet temperature to the stack were set at  $2 \times 10^{-4}$  m<sup>3</sup>/s and 15 °C respectively.

From the optimization, we selected an optimum stack configuration of five parallel lines with ten unit TEGs each in series. This resulted in a total stack power of 5523, a 110.5 W of power per unit generator. However, the maximum net power produced by the stack was 6495.7 W using a total of 260 unit TEGs, at 25 W of power per unit generator. Although there was no parasitic power penalty because of this extra weight, it seemed unreasonable to employ TEGs at such a low unit power. Inclusion of factors such as cost and space constraints would have imposed further limits on the TEG stack. However, the above optimization allowed us to select what seemed a reasonable number and arrangement of unit

TEGs in the stack for the purposes of this analysis. With this number of series and parallel generators, the exhaust and coolant flow conditions for a unit TEG in a series line are comparable to that of Case 1 at 80.5 km/h as shown in Table 4.

The aspect ratio optimization for the TEG stack using five parallel lines with each line consisting of 10 unit TEGs in series gave an optimum of 22,222 m<sup>-1</sup>. As in Case 1, Section 3.5, the number of couples and the total area for the QW module, HZQW, were assumed to be equal to those of the HZ20M.

#### 4.4. Results

##### 4.4.1. TEG power

The power produced by the TEG stack at AC generator loads of 124, 130, 137, and 143 kW is shown in Fig. 15. The error bars show the effect of AC generator efficiency on the system. At each of the AC generator loads, simulations corresponding to AC generator efficiency of 88% and 92% were performed. The TEG stack power increased slightly with AC generator load, because the exhaust mass flow rate increased with AC generator load while the coolant inlet temperature and mass flow rate were constant. The power extracted using HZQW modules was approximately 6.5–7.4 times the power extracted using HZ20M modules.

##### 4.4.2. Fuel savings

Fig. 16 shows fuel savings for Case 2. In this figure and in the following figure, the vertical ranges show the effect of AC generator efficiency on the system. The maximum fuel savings of about 3% was obtained with the HZQW module. This occurred at a AC generator load of 124 kW and efficiency of 88%.

Following the generalized fuel savings analysis in Case 1, the TEG stack power was converted to its corresponding fuel savings using the AC generator efficiency of 88% or 92% and a PCU efficiency

Table 4

A comparison of flow conditions between case studies 1 and 2.

Variable	Case 2	Case 1
exhaust flow (kg/s)	0.03	0.03
Exhaust inlet temperature (°C)	468.5	495
Exhaust outlet temperature (°C)	459	397
Coolant flow (m <sup>3</sup> /s)	$2 \times 10^{-4}$	$2 \times 10^{-4}$
Coolant inlet temperature (°C)	28.7	78
Coolant outlet temperature (°C)	29	81

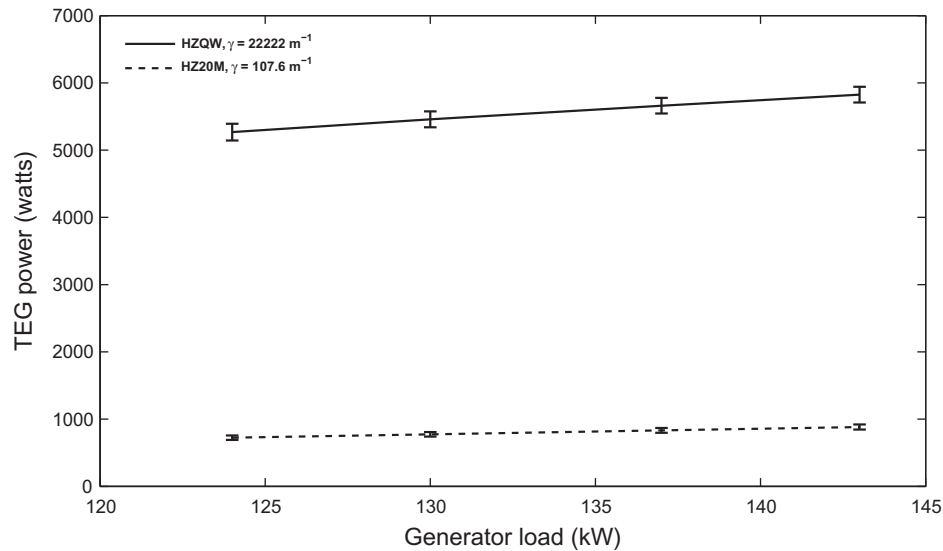


Fig. 15. TEG power production Case 2.

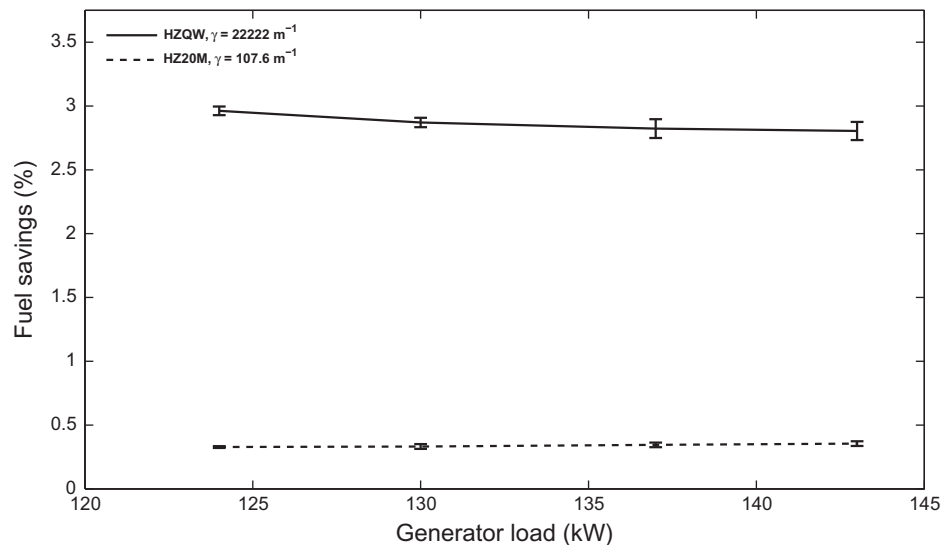


Fig. 16. Fuel savings Case 2.

of 88%. The relative fuel savings for the TEG power (HZQW) varying from 5.3 to 6 kW is about 3.2–3.3% and for the TEG power (HZ20M) varying from 0.74 to 0.9 kW is about 0.5%. These are in good agreement with the calculations based on the fuel usage from the simulations with and without the TEG, as shown in Fig. 16. This indicates that the parasitic losses were not significant, as will be verified subsequently. Also, from Fig. 16 the fuel savings, using HZQW modules, decreases with increasing AC generator load because of the decrease in power ratio as the AC generator load increased. The fuel savings using the HZ20M, also decreased as the AC generator load increased. However, this decrease was too small to appear in the figure.

The parasitic losses were evaluated as previously discussed, with that caused by weight set to zero. The parasitic blow-down power is not included because as in Case 1 necessary data was not available. The effect of back-pressure on the shaft power was accounted for as in Case 1.

Fig. 17 shows a comparison of the TEG power to the parasitic coolant pumping power and the back-pressure power. All the powers have been converted into their respective shaft powers as in

Case 1. However, the pump efficiency was not accounted for in the evaluation of parasitic pumping power. The pumping power, without accounting for the pump efficiency, was about 90 W. A pump efficiency of 25% would result in a parasitic pumping power of 360 W. These powers correspond to a range of 10–50% of the TEG stack power for the HZ20M or 1.6–7% for the HZQW. The blow-down power is again less, being at the most only 8.6% of the power generated by the TEG for HZ20M case or 1.3% for the HZQW.

#### 4.4.3. Energy budget

Table 5 compares the energy budget for the HZQW and HZ20M. The tabulations are the same as those defined in the energy budget for Case 1. From Table 5, the TEG stack efficiency due to the change in modules from HZ20M to HZQW increased by a factor of about 10. A comparison of the effectiveness for the stack shows that, already 70–66% of the maximum possible energy has been extracted using HZQW and this further increases to 96–97% using HZ20M modules. However, a significant fraction of this extracted energy is being rejected to the coolant, about 90% using HZQW and about

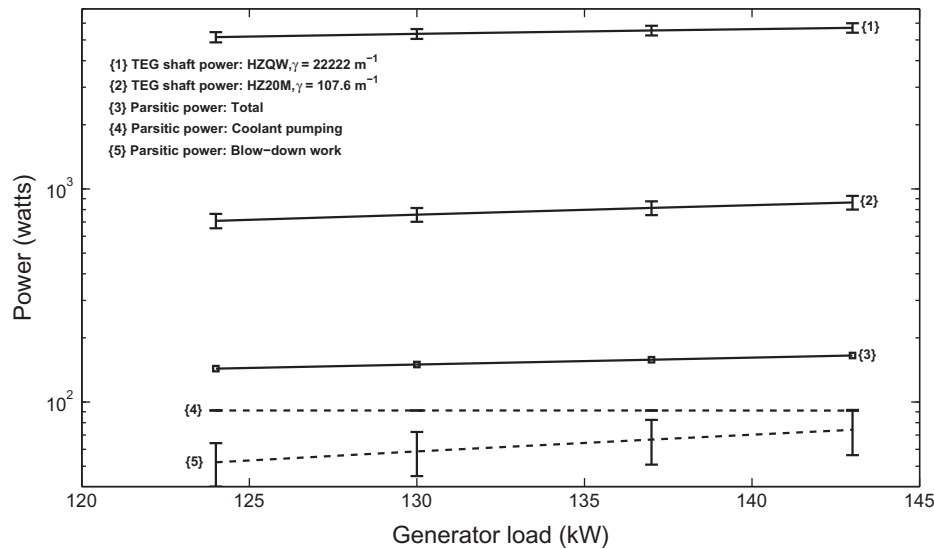


Fig. 17. Parasitic losses Case 2.

**Table 5**  
Energy budget Case 2.

AC generator load	(kW)	124	130	137	143
<b>HZQW</b>					
$\dot{W}_{e,max}$	(kW)	80.3	83.5	87.2	90.2
$\dot{W}_e$	(kW)	56.3	57.5	58.8	59.8
Effectiveness	(%)	70.1	68.8	67.4	66.3
TEG stack power	(kW)	5.27	5.46	5.66	5.83
Heat rejected to coolant	(kW)	51.0	52.0	53.1	54.0
TEG stack efficiency	(%)	9.36	9.50	9.63	9.74
<b>HZ20M</b>					
$\dot{W}_{e,max}$	(kW)	82.5	85.7	89.4	92.5
$\dot{W}_e$	(kW)	80.3	83.2	86.4	89.2
Effectiveness	(%)	97.3	97.0	96.7	96.4
TEG stack power	(kW)	0.72	0.77	0.83	0.88
Heat rejected to coolant	(kW)	79.6	82.4	85.6	88.3
TEG stack efficiency	(%)	0.90	0.93	0.96	1

99% using HZ20M modules. Any further increase in system size, though increasing the power from the stack, might not be feasible economically. In fact, with the aid of better module and heat exchanger designs the system size could be reduced while retaining the stack efficiency and effectiveness.

To summarize, the TEG stack generated about 5.3–5.8 kW using optimized QW modules. This power was greater than that of the power from  $\text{Bi}_2\text{Te}_3$  modules by a factor of 6.6–7.3. The power generated by the QW modules resulted in a fuel savings of about 3%. This stationary application allowed a larger system size and also resulted in a low total parasitic loss. The greater system size also increased the power generated, effectiveness, and efficiency of the stack.

Though the change in power generated between Cases 1 and 2 is quite large, the change in relative fuel savings is not in proportion. As discussed earlier the magnitude of power ratio, efficiency ratio, and the loss ratio determine the relative fuel savings for each of these cases. For Case 1, the power ratio for the unit TEG using HZQW modules at 112.7 km/h was about 1.3%, and the efficiency ratio,  $\eta_{CPU}/\eta_G$ , was 1.8. For Case 2 with the HZQW generator at 143 kW AC generator load, the power ratio was greater at 3.3% but the efficiency ratio was only 1.0 because of the higher-efficiency generator used. Thus, although Case 2 had a greater power ratio and a smaller loss ratio, these impacts were mitigated by the

fact that the stationary electrical generator was more efficient than the vehicle alternator.

## 5. Conclusions

The potential benefits of the application of QW and  $\text{Bi}_2\text{Te}_3$  based thermoelectric power generation from the SUV and CNG engine power generator were examined. Under both these applications the QW based TEG generated more power relative to the  $\text{Bi}_2\text{Te}_3$  based TEG. For the SUV, the QW based TEG generated about 100–450 W, which should result in a fuel savings of about 2–2.3%. However, the fuel savings decreased by about 30%, primarily due to the rolling resistance parasitic loss. In contrast, for the CNG case the total parasitic loss was low relative to the TEG stack power. This was primarily because this was a stationary application and the lack of space constraint has allowed an increase in system size. The optimized QW based TEG stack generated about 5.3–5.8 kW resulting in a fuel savings of about 3%. The low relative fuel gains despite the higher TEG stack power and lower parasitic loss was primarily due to the high efficiency of the electrical generator. The energy budget showed that, under both the applications, a significant fraction of the exhaust energy was rejected to the coolant.

## Acknowledgement

This work was sponsored by the New York State Energy Research and Development Authority under Agreement 6642.

## References

- [1] Hicks L, Dresselhaus M. Use of quantum-well superlattices to obtain a high figure of merit from nonconventional thermoelectric materials. In: Proceedings of the 1993 MRS fall meeting, vol. 326. Boston, MA (USA); 1994. p. 413–8.
- [2] Fleurial J-P, Borshchevsky A, Caillat T, Morelli DT, Meisner GP. High figure of merit in Ce-filled skutterudites. In: Proceedings of the fifteenth international conference on thermoelectrics, Pasadena, CA (USA); 1996. p. 91–5.
- [3] Tavkhelidze A. Large enhancement of the thermoelectric figure of merit in a ridged quantum well. Nanotechnology 2009;20(40):405401.
- [4] Ghamaty S, Elsner N. Development of quantum well thermoelectric device. In: Proceedings of the eighteenth international conference on thermoelectrics, Baltimore, MD (USA); 1999. p. 485–8.
- [5] Jovanovic V, Ghamaty S, Elsner NB. Design, fabrication, and testing of quantum well thermoelectric generator. In: Proceedings of the tenth intersociety conference on thermal and thermomechanical phenomena in electronics systems, San Diego CA (USA); 2006. p. 1417–23.

- [6] Ghamaty S, Elsner N. Si/SiGe quantum well thermoelectric materials and devices for waste heat recovery from vehicles and industrial plants. In: Proceedings of the international symposium on nano-thermoelectrics, Osaka, Japan; 2007.
- [7] Thacher EF, Helenbrook BT, Karri MA, Richter CJ. Testing an automobile exhaust thermoelectric generator in a light truck. *Proc IMechE, Part D: J Automobile Eng* 2007;221(D1):95–107.
- [8] El-Genk M, Saber H, Caillat T, Sakamoto J. Tests results and performance comparisons of coated and un-coated skutterudite based segmented unicouples. *Energy Convers Manage* 2006;47(2):174–200.
- [9] Saber HH, El-Genk MS, Caillat T. Tests results of skutterudite based thermoelectric unicouples. *Energy Convers Manage* 2007;48(2):555–67.
- [10] Saber HH, El-Genk MS. Effects of metallic coatings on the performance of skutterudite-based segmented unicouples. *Energy Convers Manage* 2007;48(4):1383–400.
- [11] Hendricks TJ. Thermal system interactions in optimizing advanced thermoelectric energy recovery systems. *J Energy Resour Technol – Trans ASME* 2007;129(3):223–31.
- [12] Hendricks TJ. Comparison of skutterudites and advanced thin-film B4C/B 9C and Si/SiGe materials in advanced thermoelectric energy recovery systems. In: Proceedings of the twenty-fourth international conference on thermoelectrics, Clemson, SC (USA); 2005. p. 369–75.
- [13] Hendricks TJ, Lustbader JA. Advanced thermoelectric power system investigations for light-duty and heavy duty applications: part II. In: Proceedings of the twenty-first international conference on thermoelectrics, Long Beach, CA; 2002. p. 387–94.
- [14] Hendricks TJ, Lustbader JA. Advanced thermoelectric power system investigations for light-duty and heavy duty applications: part I. In: Proceedings of the twenty-first international conference on thermoelectrics, Long Beach, CA; 2002. p. 381–6.
- [15] Hendricks TJ. Optimum design parameters in two-stage thermoelectric generators. In: Proceedings of the twenty-third intersociety energy conversion engineering conference, A89-15176 04-44. Denver (CO): American Society of Mechanical Engineers; 1988. p. 339–45.
- [16] Esarte J, Min G, Rowe D. Modelling heat exchangers for thermoelectric generators. *J Power Sources* 2001;93(1–2):72–6.
- [17] Rowe D, Min G. Evaluation of thermoelectric modules for power generation. *J Power Sources* 1998;73(2):193–8.
- [18] Rowe DM. Development of improved modules for the economic recovery of low temperature waste heat. In: Proceedings of the sixteenth international conference on thermoelectrics, Dresden, Germany; 1997. p. 532–8.
- [19] Rowe D, Min G. Design theory of thermoelectric modules for electrical power generation. *IEE Proc – Sci Meas Technol* 1996;143(6):351–6.
- [20] Min G, Rowe D. Optimisation of thermoelectric module geometry for “waste heat” electric power generation. *J Power Sources* 1992;38(3):253–9.
- [21] Chen M, Lu S, Liao B. On the figure of merit of thermoelectric generators. *J Energy Resour Technol – Trans ASME* 2005;127(1):37–41.
- [22] Crane D, Jackson G. Systems-level optimization of low-temperature thermoelectric waste heat recovery. In: Pierson E, Jackson WD, editors. Proceedings of the 37th intersociety energy conversion engineering conference (IECEC), Washington, DC (USA); 2002. p. 583–8.
- [23] Wu C. Analysis of waste-heat thermoelectric power generators. *Appl Thermal Eng* 1996;16(1):63–9.
- [24] DiSalvo FJ. Thermoelectric cooling and power generation. *Science* 1999;285(5428):703–6.
- [25] Crane D, Jackson G. Optimization of cross flow heat exchangers for thermoelectric waste heat recovery. *Energy Convers Manage* 2004;45(9–10):1565–82.
- [26] Fairbanks JW. Thermoelectric developments for vehicular applications. In: Diesel engine-efficiency and emissions research conference, Detroit, MI (USA); 2006.
- [27] Willigan R. Cost-effective fabrication routes for the production of quantum well type structures and recovery of waste heat from heavy duty trucks. In: Diesel engine-efficiency and emissions research conference, Detroit, MI (USA); 2006.
- [28] Brooker A. Advisor documentation, Tech. rep., National Renewable Energy Laboratory; 2002.
- [29] Karri MA. Modeling of an automotive exhaust thermoelectric generator. Master's thesis, Clarkson University, Department of Mechanical and Aeronautical Engineering, Potsdam, NY; 2005.
- [30] Hi-Z Technology, HZ-20 product brochure.
- [31] Angrist SW. Direct energy conversion. Boston, MA (USA): Allyn and Bacon Inc.; 1971.
- [32] Ghamaty S. Quantum well thermoelectrics for converting waste heat to electricity. In: Quarterly tech. rep., Department of Energy Award: DE-FC26-03NT41974. San Diego, CA: Hi-Z Technology, Inc.; 2004.
- [33] Wilke CR. A viscosity equation for gas mixtures. *J Chem Phys* 1950;18(4):517–9.
- [34] Prestone, Prestone antifreeze coolant properties, personal communication; 2003.
- [35] Manglik RM, Bergles AE. Heat transfer and pressure drop correlations for the rectangular offset strip fin compact heat exchanger. *Exp Thermal Fluid Sci* 1995;10:171–80.
- [36] Dittus FWL, Boelter MK. Heat transfer in automobile radiators of the tubular type. *Univ Calif Publ Eng* 1930;2(13):443–61.
- [37] Vazquez J, Sanz-Bobi MA, Palacios R, Arenas A. State of the art of thermoelectric generators based on heat recovered from the exhaust gases of automobiles. In: Proc 7th European workshop on thermoelectrics, Pamplona, Spain; 2002.
- [38] Hauerbach M, personal communication. Hi-Z Technology, Inc.; 2005.
- [39] Sangwan K, personal communication. Delphi Corporation; 2004.
- [40] Graham C, personal communication. General Motors Corporation; 2002.
- [41] Richter CJ, personal communication. Delphi Corporation, January 2004.
- [42] White FM. Fluid mechanics. McGraw Hill; 2003.
- [43] Krommenhoek D, personal communication. Hi-Z Technology, Inc.; 2008.
- [44] Krommenhoek D, personal communication. Hi-Z Technology, Inc.; 2005.
- [45] John Deere power tech 6068h diesel engine for generator set applications specifications; 2008.